Stem Cell Reviews and Reports (2023) 19:170–187
https://doi.org/10.1007/s12015-022-10408-x

LncRNA RAD51-AS1 Regulates Human Bone Marrow Mesenchymal Stem Cells via Interaction with YBX1 to Ameliorate Osteoporosis

Beichen Li[1] · Jing Wang[2] · Fangrong Xu[2] · Qinjue Wang[1] · Quan Liu[1] · Guantong Wang[1] · Dengshun Miao[2,3] · Qiang Sun[1]

Accepted: 30 May 2022 / Published online: 21 June 2022

Abstract

Long noncoding RNA (lncRNA) is a new key regulatory molecule in the occurrence of osteoporosis, but its research is still in the primary stage. In order to study the role and mechanism of lncRNA in the occurrence of osteoporosis, we reannotated the GSE35956 datasets, compared and analyzed the differential expression profiles of lncRNAs between bone marrow mesenchymal stem cells (hBMSCs) from healthy and osteoporotic patients, and then screened a lncRNA RAD51-AS1 with low expression in hBMSCs from osteoporotic patients, and its role in the occurrence of osteoporosis has not been studied. We confirmed that the expression level of lncRNA RAD51-AS1 in hBMSCs from patients with osteoporosis was significantly lower than those from healthy donors. A nuclear cytoplasmic separation experiment and RNA fluorescence in situ hybridization showed that RAD51-AS1 was mainly located in the nucleus. RAD51-AS1 knockdown significantly inhibited the proliferation and osteogenic differentiation of hBMSCs and significantly increased their apoptosis, while RAD51-AS1 overexpression significantly promoted the proliferation, osteogenic differentiation, and ectopic bone formation of hBMSCs. Mechanistically, we found that RAD51-AS1 banded to YBX1 and then activated the TGF-β signal pathway by binding to Smad7 and Smurf2 mRNA to inhibit their translation and transcription up-regulated PCNA and SIVA1 by binding to their promoter regions. In conclusion, RAD51-AS1 promoted the proliferation and osteogenic differentiation of hBMSCs by binding YBX1, inhibiting the translation of Smad7 and Smurf2, and transcriptionally up-regulated PCNA and SIVA1.

Keywords LncRNA · Osteoporosis · Human Bone Marrow Mesenchymal Stem Cells · RAD51-AS1 · YBX1

Introduction

Osteoporosis is an unbalanced internal microenvironment characterized by a decrease in bone density and bone mass, and the destruction of the bone microarchitecture, resulting in increasing bone brittleness and a higher chance of fragility fractures [1–3]. Fractures from osteoporosis become increasingly common in women after 55 years of age and men after 65 years of age, contributing substantially to bone-associated morbidities/mortality and increased healthcare costs [4–6]. The situation has prompted global efforts to find more effective strategies for preventing and treating osteoporosis.

Bone marrow mesenchymal stem cells (BMSCs) are pluripotent stem cells with the ability to self-renew and the potential for multilineage differentiation [7]. Under certainly induced microenvironments, BMSCs can differentiate into various cell types, including osteoblasts, adipocytes, and chondrocytes [8, 9]. Furthermore, it is solidly established by the research of Benedetto Sacchetti and others that the self-renewal of progenitors within the BMSC population [10]. Recent studies have shown that the abnormal differentiation of BMSCs, especially the imbalance between osteogenic and adipogenic differentiation, plays a crucial role in osteoporosis [11–13]. In addition, the regulation of proliferation

✉ Dengshun Miao
dsmiao@njmu.edu.cn

✉ Qiang Sun
sunqiang_cn@njmu.edu.cn

[1] Department of Orthopedics, Nanjing First Hospital, Nanjing Medical University, Nanjing 210006, China

[2] State Key Laboratory of Reproductive Medicine, Department of Anatomy, Histology and Embryology, The Research Center for Bone and Stem Cells, Nanjing Medical University, Nanjing 211100, China

[3] Department of Plastic Surgery, The Affiliated Friendship Plastic Surgery Hospital of Nanjing Medical University, Nanjing 211161, China

and apoptosis of BMSCs is one of the key factors affecting osteoporosis [14, 15]. Therefore, identifying a critical target associated with the function of BMSCs would greatly facilitate the early diagnosis and treatment of the disease.

Long noncoding RNAs (lncRNAs), defined as transcripts of > 200 nucleotides with little or no protein-coding potential [16], regulate various diseases and biological processes, including cellular proliferation, apoptosis, differentiation, and gene regulation [17, 18]. The mechanism of lncRNAs can be classified into four modes: signal, decoy, guide, and scaffold [19]. LncRNAs can regulate histone modifications, chromatin remodeling, protein functional activities, and RNA metabolism by acting in cis or trans. Further, they are widely involved in epigenetics, transcription, and post-transcriptional regulation [20, 21]. There is now increasing evidence for the involvement of lncRNAs in the progression of osteoporosis. For example, the lncRNA Bmncr serves as a scaffold to facilitate the interaction of TAZ and ABL to form the TAZ and RUNX2/PPARG transcriptional complex assembly, promoting osteogenesis and inhibiting adipogenesis [22]. The lncRNA Nron regulates the stability of ERα in osteoclasts via interaction with the E3 ligase CUL4B through the functional motif [23]. The lncRNA GAS5 targets the UPF1/SMAD7 axis and protects against osteoporosis to promote osteoblast differentiation [24]. However, there are still no reports on the associations between RAD51-AS1 and osteoporosis.

In the current study, we assumed that RAD51-AS1 may function with an RNA-binding protein (RBP) and further investigate the role and molecular mechanism of RAD51-AS1 in hBMSCs. Our report may unanimously support the hypothesis that lncRNA RAD51-AS1 may be a novel target in osteoporosis by interacting with an RBP in hBMSCs.

Materials and Methods

LncRNA Reannotation

The Affymetrix HG-U133Plus 2.0 microarray was used in the GSE35956 datasets, including 54,675 probe sets. We developed a lncRNA annotation pipeline to identify the probe sets mapped to lncRNAs. First, we downloaded the HG-U133 Plus 2.0 microarray probe annotations from the Affymetrix website to filter the probe sets with Refseq IDs, labeled as "NR_" or "XR_". Second, we combined the GSE35956 matrix with the Step 1 file with the probe ID. Third, the Step 2 file was combined with the annotation file by the Symbol, which we achieved from the Genecode database (https://www.gencodegenes.org). Therefore, in total, specific 1,228 annotated lncRNA transcripts with corresponding Affymetrix probe IDs were selected [25].

Microarray Analysis

GSE35956 raw data were downloaded from The Gene Expression Omnibus (GEO) database (GSE35956). Background correction and normalization of the data microarray were processed by the Affy installation package of R software. Furthermore, the specific 1,228 lncRNA expression matrix was generated using R software based on the normalized expression. The differential gene expression analysis was performed by the limma R package. A volcano was drawn on the dif-lncRNA using the ggplot R package.

Cell Isolation and Culture

After obtaining informed consent from volunteers at the Nanjing First Hospital (Nanjing, Jiangsu Province, People's Republic of China), human bone marrow mesenchymal stem cells (hBMSCs) were isolated from bone marrow. Briefly, the bone marrow was extracted from the spinal vertebrae under sterile conditions. hBMSCs were purified, isolated, and cultured using Ficoll density gradient centrifugation methods. HBMSCs in passage two were used in the experiments. HBMSCs were cultivated in α-minimum essential medium (Gibco, Grand Island, NY) blended with 5% UltraGRO (Helios BioScience), and 100 mg/L streptomycin (Gibco). The study was approved by the ethics committee of the Nanjing First Hospital (Nanjing, Jiangsu Province, People's Republic of China). After explaining the research in detail, the possible risks and importance, as well as informing methods of privacy protection, we obtained informed consent and published signatures of all patients or normal donors.

RNA Extraction and Real-Time qPCR

Total RNA was extracted from hBMSCs and bone tissues using TRIzol reagent (Invitrogen, Life Technology, USA) following the manufacturer's instructions. The total RNA samples of 1 μg each were used to perform the next reverse transcription. cDNA was generated using the HiScript II Q RT SuperMix for qPCR (Vazyme, China). The following cycling profile was used: 50 °C for 15 min, 85 °C for 5 s, and cooling at 4 °C. The amplification reactions were assembled in a 10 μL reaction volume containing 5 μL of ChamQ SYBR qPCR Master Mix (Vazyme, China), 3.6 μL of double-distilled water, 0.4 μL of amplification primers, and 1 μL of cDNA in each amplification reaction, by using a Roche LightCycler 480 PCR machine. Gene expression analysis was calculated by the $2^{-\Delta\Delta CT}$ method. The forward and reverse primers for each gene are listed in Table S1.

Nuclear and Cytoplasmic Fractionation

Nuclear and cytoplasmic RNA was extracted as described previously and in accordance with the manufacturer's instructions (PARIS, Part Number AM1921). Cells were lysed in lysis solution and isolated in cell disruption and cell fractionation buffer. The expression of lncRNA RAD51-AS1 in each of the fractions was determined by real-time qPCR. The data were analyzed to determine the nuclear and cytoplasmic levels of hBMSCs.

Cell Transfection

The Smart Silencer of lncRNA RAD51-AS1, purchased from Ribobio (Guangzhou, China), contains three siRNA and three ASOs to avoid off-target effects and improve transfection efficiency. PcDNA3.1-RAD51-AS1 came from General (Shanghai, China). Lipofectamine 3000 (Invitrogen, Carlsbad, CA, USA) and 100 nM oligonucleotide were incubated in one tube and transfected for 15 min.

Osteogenic Differentiation of hBMSCs

For osteoblast differentiation, hBMSCs were cultured in the osteoblast differentiation medium (α-MEM containing 5% UltraGRO, 1 μM dexamethasone, 10 mM β-glycerol phosphate, 50 μM ascorbic acid, 100 IU/mL penicillin, and 100 IU/mL streptomycin) for 5 days. The medium was replaced every 3 days.

Lentiviral Vector Construction and Transfection

The packaged RAD51-AS1 overexpressing lentivirus vector and knockdown vector were obtained from Genechem (Shanghai, China) to generate the lentivirus. All lentivirus vectors were used for hBMSCs transfection at an MOI of 20–30. HBMSCs were plated at a density of 3×10^5–5×10^5 cells/cm^2 in each 6-well plate (Corning, USA). When hBMSCs grew to 50%–60% confluence, the transfection was performed at the appropriate volume of fresh α-Minimum (Gibco, Grand Island, NY) without UltraGRO to improve efficiency, in accordance with the manufacturer's instructions. After reaction for 6 h, the medium was refreshed. The transfection efficiency of the lentivirus was verified by real-time qPCR.

Cell Viability and Apoptosis Assays

The MTT assay (Biofroxx, Germany) was used to assay cell proliferation. In 96-well plates, the cells were seeded at 3×10^3 cells per well. A spectrophotometric plate reader set at 490 nm was used to measure cell viability. The TUNEL assay using the riboAPO One-Step TUNEL Apoptosis Kit (Ribobio, Guangzhou, China) was performed to assess apoptosis following the manufacturer's protocol. Cells were co-stained with DAPI to visualize the nuclei.

EdU Assay

The EdU cell proliferation assay kit (Ribobio, Guangzhou, China) was used for the hBMSCs proliferation assay. Briefly, cells were incubated in Chamber Slide (Thermo Scientific, USA) with 50 μM EdU labeling medium at 37 °C for 12 h. After immobilization and coupling with Hoechst 33,342 staining, the cells were observed under a fluorescence microscope. More than five random fields per well were captured, and the corresponding cells were counted.

ALP Staining

ALP staining (Beyotime, Shanghai, China) was performed on day 5. In brief, the cells were fixed with 4% paraformaldehyde for 30 min, washed with PBS three times for 5 min, and mixed with the appropriate amount of BCIP/NBT staining liquid to stain hBMSCs. HBMSCs were incubated at room temperature for 20–30 min. Then, the working fluid was removed, and hBMSCs were washed twice with distilled water to stop the reaction.

Ectopic Bone Formation of hBMSCs In Vivo

The animal plan was finally approved by the Animal Use and Care Committee of the Nanjing Medical University. Eight-week-old BALB/c homozygous nude (nu/nu) mice were purchased from Ziyuan Laboratory Animal Technology Co., Ltd. (Zhejiang, China). Mice were randomly divided into the vector group (vector, n = 5) and the RAD51-AS1 group (RAD51-AS1, n = 5). HBMSCs were transfected with lentiviruses (pcDNA3.1 or oe-RAD51-AS1-1) and were cultured in the osteoblast medium for 7 days prior to the in vivo study. The cells (5×10^5) were resuspended and planted onto a 2.5*2.5*2.5 mm β-Tricalcium phosphate (β-TCP) scaffold. Then, the scaffolds were implanted subcutaneously into the backs of 8-week-old BALB/c homozygous nude (nu/nu) mice. The implants were removed after 8 weeks and fixed in 4% paraformaldehyde. HE staining, Masson staining, and immunohistochemistry were performed subsequently.

Western Blotting and Antibodies

Cells and tissues were lysed in RIPA lysis buffer containing a protease inhibitor cocktail. Protein lysates were separated by SDS polyacrylamide gel electrophoresis (SDS-PAGE) and transferred onto PVDF membranes. Non-specific binding to the membranes was blocked by incubation with 5% milk and then subsequently incubated with primary antibodies against

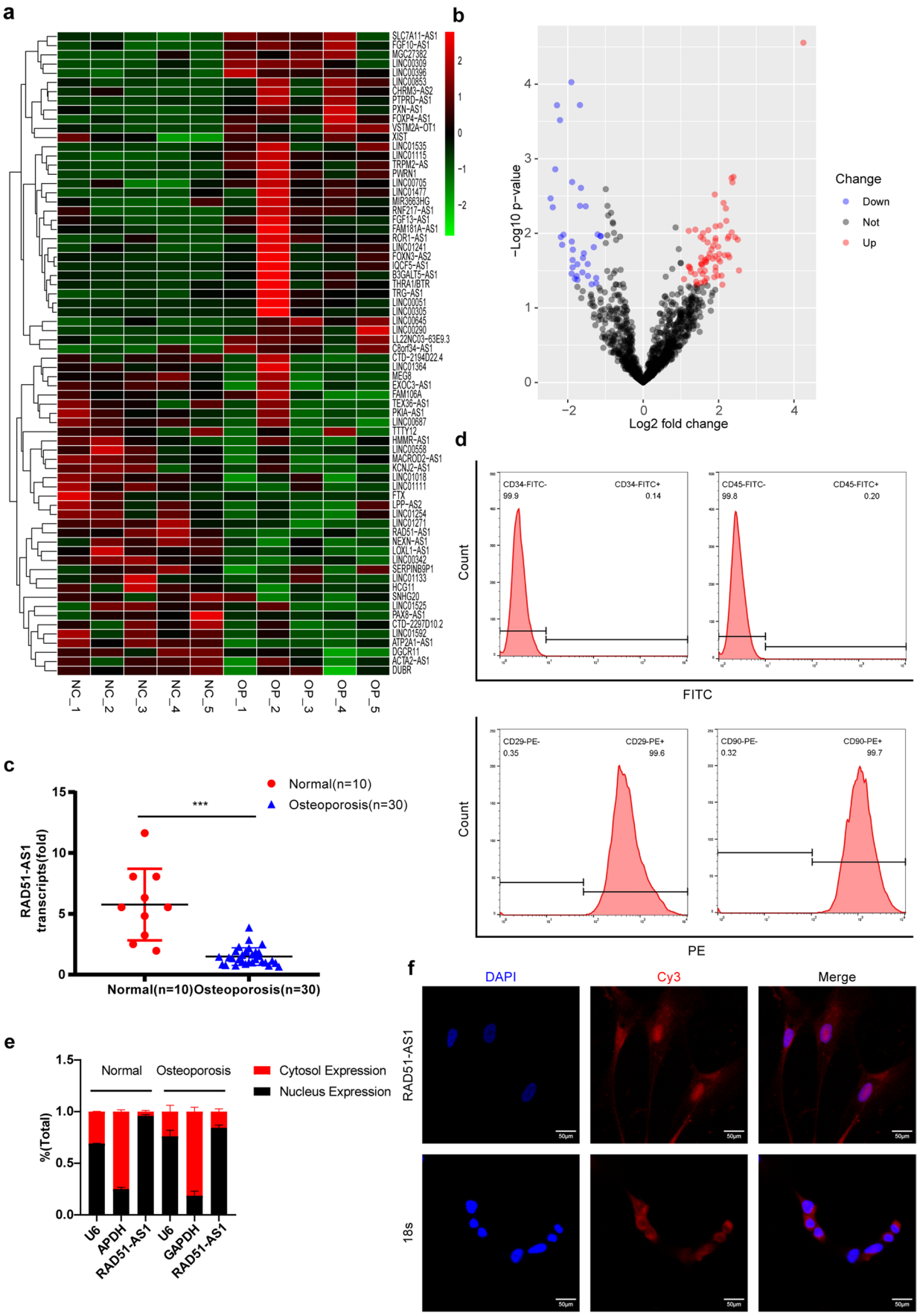
a
SLC7A11-AS1
FGF10-AS1
MGC27382
LINC00309
LINC00396
LINC00853
CHRM3-AS2
PTPRD-AS1
PXN-AS1
FOXP4-AS1
VSTM2A-OT1
XIST
LINC01535
LINC01115
TRPM2-AS
PWRN1
LINC00705
LINC01477
MIR3663HG
RNF217-AS1
FGF13-AS1
FAM181A-AS1
ROR1-AS1
LINC01241
FOXN3-AS2
IQCF5-AS1
B3GALT5-AS1
THRA1/BTR
TRG-AS1
LINC00051
LINC00305
LINC00645
LINC00290
LL22NC03-63E9.3
C8orf34-AS1
CTD-2194D22.4
LINC01364
MEG8
EXOC3-AS1
FAM106A
TEX36-AS1
PKIA-AS1
LINC00687
TTTY12
HMMR-AS1
LINC00558
MACROD2-AS1
KCNJ2-AS1
LINC01018
LINC01111
FTX
LPP-AS2
LINC01254
LINC01271
RAD51-AS1
NEXN-AS1
LCKL1-AS1
LINC00342
SERPINB9P1
LINC01133
HCG11
SNHG20
LINC01525
PAX8-AS1
CTD-2297D10.2
LINC01592
ATP2A1-AS1
DGCR11
ACTA2-AS1
DUBR
NC_1
NC_2
NC_3
NC_4
NC_5
OP_1
OP_2
OP_3
OP_4
OP_5
2
1
0
-1
-2
b
−Log10 p−value
Log2 fold change
Change
Down
Not
Up
c
Normal(n=10)
Osteoporosis(n=30)
***
RAD51-AS1 transcripts(fold)
Normal(n=10)Osteoporosis(n=30)
d
CD34-FITC-
99.9
CD34-FITC+
0.14
CD45-FITC-
99.8
CD45-FITC+
0.20
Count
FITC
CD29-PE-
0.35
CD29-PE+
99.6
CD90-PE-
0.32
CD90-PE+
99.7
Count
PE
e
Normal
Osteoporosis
Cytosol Expression
Nucleus Expression
%(Total)
U6
APDH
RAD51-AS1
U6
GAPDH
RAD51-AS1
f
DAPI
Cy3
Merge
RAD51-AS1
18s
50μm

◂**Fig. 1** Filtering of RAD51-AS1 by bioinformatics analysis. **a, b** Raw microarray data were downloaded from the GEO dataset (GSE35956), including healthy individuals (n = 5) and patients with osteoporosis (n = 5). **a** Raw data are shown with the top 35 DE lncRNAs presented as a heatmap. **b** Raw data are shown with the cutoff fold-changes of ≥ 1 or ≤ − 1 and $p < 0.05$ on a volcano plot. **c** RAD51-AS1 expression in patients with osteoporosis (n = 30) compared with normal individuals (n = 10) via RT-qPCR. **d** Surface markers on hBMSCs were identified by flow cytometry using FITC-labeled CD34 and CD45 and PE-labeled CD29 and CD90. **e** After nuclear and cytoplasmic fractionation, RNA expression levels were measured by qRT-PCR. GAPDH was used as a cytosol marker; U6 was used as a nuclear marker (n = 3). **F** RAD51-AS1 RNA FISH was performed in HBMSCs via cy3-labeled probes (n = 3). *$p < 0.05$, ** $p < 0.01$, and *** $p < 0.001$

YBX1 (1:1000, ab76149, Abcam), SMURF2 (1:1000, ab53316, Abcam), and SMAD7 (1:1000, 66,478–1-Ig, Proteintech) at 4 °C overnight. The membrane was washed with TBST buffer and then incubated with appropriate secondary antibodies at room temperature for 1 h. The protein levels were detected using ImageJ software (NIH, USA).

Chromatin Isolation by RNA Purification (CHIRP) Assay for Protein and Mass Spectrometry

The CHIRP assay was performed using the Target RNA Purification Kit (Shanghai Zeheng Biotech, China) as described previously, but with minor modifications [26]. The probes used were synthesized by Genscript (Nanjing, China), and are listed in Table S2. The cells were crosslinked by formaldehyde, equilibrated in glycine buffer, and scraped with lysis buffer. Cell samples were sonicated and then centrifuged. The supernatant was transferred to a 2 mL tube and 50 µL was saved separately as the input analysis. Cell lysates were incubated with the biotin-tagged specific probe or control probe for 3 h. The supernatant lysate was incubated with streptavidin beads for 1 h with rotating. The beads/sample mixture was washed. Subsequently, 10% of the beads/sample mixture was re-purified by TRIzol. Purified mRNA was detected by qRT-PCR. First, 90% of the beads/sample mixture was resuspended in protein buffer and heated at 100℃ for 5 min. The RBPs were sequenced and identified by LC–MS/MS, as described by the EASY-nano-LC system (Thermo Scientific, MA, USA).

Fluorescent In Situ Hybridization (FISH) and Immunofluorescence (IF)

For RNA FISH, a Ribo Fluorescent In Situ Hybridization Kit (Ribobio, Guangzhou, China) was performed to detect the lncRNA RAD51-AS1 in hBMSCs. In brief, the cells in the wells were fixed with 4% polyoxymethylene for 20 min, permeabilized, and prehybridized in hybridization buffer, and then hybridized at 55 °C for 1 h with a RAD51-AS1 probe mix (Ribobio, Guangzhou, China), and modified with Cy5. Images were obtained using an LSM 5 Exciter confocal imaging system (Carl Zeiss).

For FISH and IF double staining, the anti-YBX1 primary antibody (1:100, ab76149, Abcam) was added overnight at 4℃ after completing the FISH procedure. Finally, the CoraLite488-labeled fluorescent secondary antibody (1:800, SA00013-2, Proteintech) was added and detected.

RNA Immunoprecipitation (RIP)

RIP was performed using the RIP kit produced by Geneseed (Guangzhou, China). In brief, 1×10^7 cells were harvested by RIP lysis buffer and then incubated with RIP buffer containing magnetic beads conjugated to anti-YBX1 antibodies. Purified rabbit IgG was used as a negative control. The immunoprecipitated RNAs were isolated and purified for real-time qPCR analysis to detect the presence of the target mRNA.

Cleavage Under Targets and Tagmentation (CUT&Tag) Assay

The CUT&Tag assay was performed using the NovoNGS® CUT&Tag 3.0 High-Sensitivity Kit (NovoProtein, Shanghai, China). First, 5.0×10^5 hBMSCs cells were washed twice with 1.5 mL of wash buffer and then mixed with activated concanavalin A beads. After successive incubations with the primary antibody (anti-YBX1, room temperature, 2 h) and secondary antibody (room temperature, 1 h), the cells were washed and incubated with pAG-Tn5 for 1 h. Then, $MgCl_2$ was added to activate tagmentation for 1 h. The tagmentation reaction was stopped, and the chromatin complex was digested with a solution containing 10 µL of 0.5 M EDTA, 3 µL of 10% SDS, and 2.5 µL of 20 mg/mL proteinase K at 55 °C for 10 min. The transposed DNA fragments were extracted and purified by using the DNA beads (NovoProtein, Shanghai, China). The libraries were sequenced by using the Illumina NovaSeq 6000 platform.

The trimmed sequencing reads (trim_galore) were aligned to the reference human genome (GRCh37/hg19) using BOWTIE2 with very sensitive parameters. The peaks were called using MACS2. A heatmap was generated using deepTools.

Statistical Analysis

Each experimental procedure involving cells was repeated at least three times. All data were expressed as the mean ± standard deviation (SD). Statistical analysis

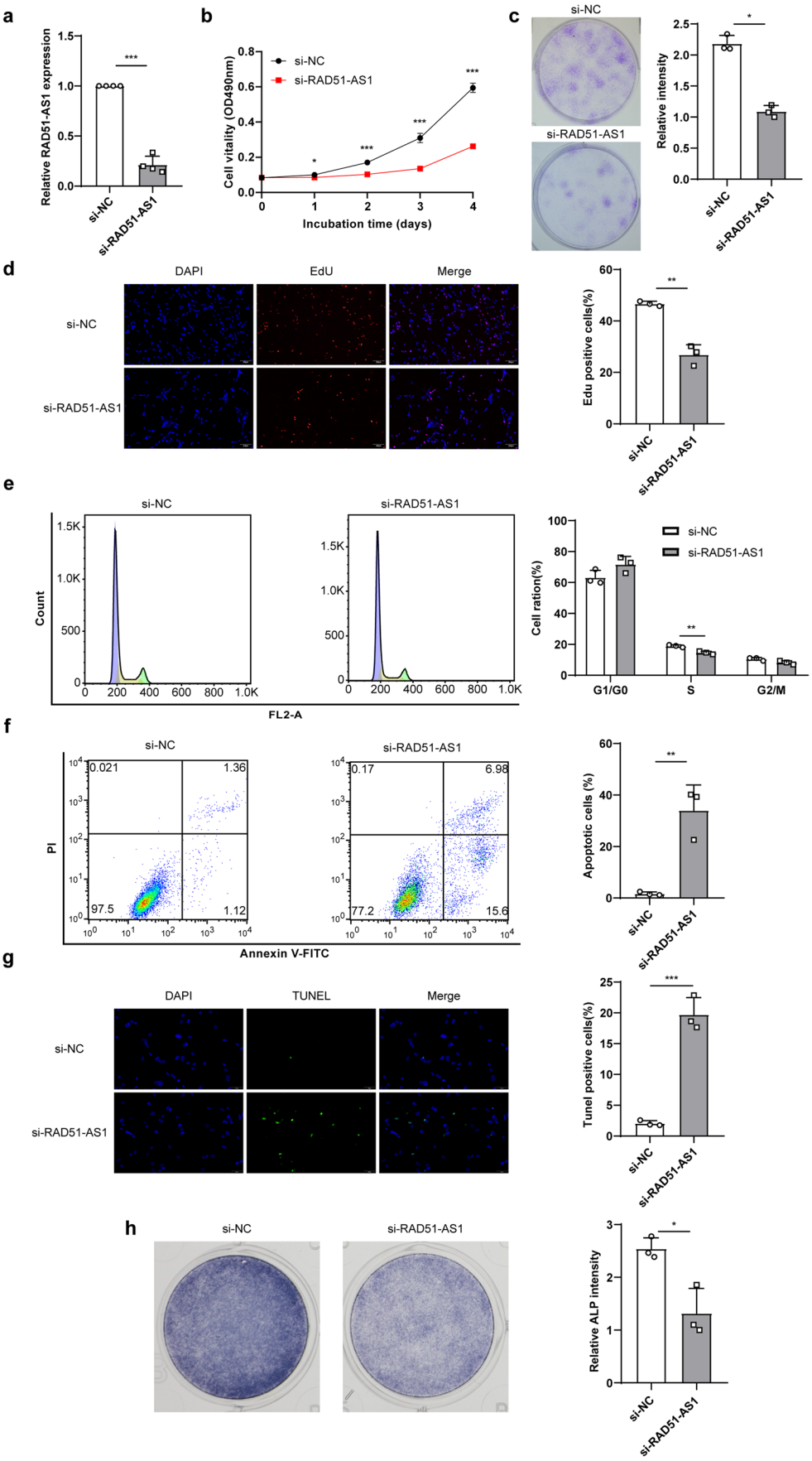

Fig. 2 Effects on hBMSCs after silencing of RAD51-AS1. **a** RT-qPCR was used to measure the silencing efficiency of si-RAD51-AS1 (n = 4). **b** The MTT assay was performed to determine cell proliferation of hBMSCs after transfection of si-RAD51-AS1 (n = 3). **c** The colony formation assay was performed after transfection of si-RAD51-AS1 to determine the colony-forming ability of transfected hBMSCs (n = 3). **d** The Edu assay was used to detect the cell proliferation after transfection of si-RAD51-AS1. The positive points were counted and captured (n = 3). **e** At 48 h after transfection of si-RAD51-AS1, the cell cycle was analyzed by flow cytometry. The bars indicate the percentages of cells in the G1/G0 phase, S phase, or G2/M phase, as shown in the chart (n = 3). **f** At 48 h after transfection, hBMSCs were stained and analyzed by flow cytometry. Apoptotic cells include early and terminal apoptotic cells (n = 3). **g** The Tunel assay was used to detect apoptotic cells after transfection of si-RAD51-AS1. The positive points were counted and captured (n = 3). **h** ALP staining in the si-RAD51-AS1 or si-NC group (n = 3). *p < 0.05, ** p < 0.01, and *** p < 0.001

was performed using SPSS 18.0 software (SPSS, Chicago, IL, USA). We use the Shapiro–Wilk test to test the normality of the distribution. Statistical differences were analyzed by two-tailed Student's *t*-test for other comparisons. Analysis of variance (ANOVA) and appropriate post hoc analyses were used for comparisons of more than two groups. When a normal data distribution could not be assured, the Wilcoxon/Mann–Whitney test was applied. A probability value of 0.05 or less was considered statistically significant.

Results

LncRNA RAD51-AS1 was Downregulated Significantly in hBMSCs and Mainly Localized in the Nuclei

GSE35956 microarray data entries were retrieved from the GEO database for osteoporosis to research the differentially expressed lncRNAs in osteoporosis. The GSE35956 is a dataset for osteoporosis that includes ten BMSC samples: five from healthy controls and five from patients with osteoporosis. Based on previous papers, we performed lncRNA re-annotation on the GPL570 platform microarray [25]. We analyzed differently expressed (DE) lncRNAs with the cutoff fold-changes of ≥ 1 or ≤ -1 and $p < 0.05$ in the normal and osteoporosis groups. The results identified 103 DE lncRNAs (68 upregulated and 35 downregulated) in the osteoporosis group compared with the normal group; the DE lncRNAs are shown in Table S3. The DE lncRNAs in the samples are presented as a heatmap (Fig. 1a) and a volcano plot (Fig. 1b). We then chose three lncRNAs that had not been researched in previous studies and were highly expressed in hBMSCs derived from the normal donors but were down-regulated in hBMSCs derived from the osteoporosis patients. After qPCR verification in hBMSCs extracted from healthy controls and patients with osteoporosis, we found that the expression levels of lncRNA RAD51-AS1 were significantly down-regulated in hBMSCs derived from the osteoporosis patients compared with those derived from the normal donors (Fig. 1c). Therefore, we choose lncRNA RAD51-AS1 for this study.

The identity of HBMSCs was confirmed from the immunophenotype profile. The cells used in the experiments were positive for the hBMSCs surface antigens CD29-phycoerythrin (PE), CD90-PE, and negative for CD34-fluorescein isothiocyanate (FITC) and CD45-FITC (Fig. 1d) [27, 28]. The correct separation of the cells is crucial for the subsequent experiments.

To explore the expression distribution of RAD51-AS1, we performed nuclear and cytoplasmic fractionation. As shown in the picture (Fig. 1e), RAD51-AS1 was predominantly expressed in the nucleus in both the healthy controls and patients with osteoporosis. The locations of RAD51-AS1 and the nucleus in hBMSCs were shown to co-locate via RNA-FISH (Fig. 1f), further indicating that RAD51-AS1 was mainly expressed in the hBMSC nuclei.

Knockdown of RAD51-AS1 Promoted Apoptosis but Attenuated Cell Viability and Osteogenic Differentiation in hBMSCs

To achieve better knockdown RAD51-AS1 and reduce off-target effects, we used Smart Silencer, which contains three siRNA and three ASOs. The Smart Silencer-mediated knockdown was used for the exogenous manipulation of the RAD51-AS1 expression in hBMSCs (Fig. 2a). To explore the role of RAD51-AS1 in hBMSCs, MTT assays showed that the knockdown of RAD51-AS1 expression significantly inhibited cell viability compared with transfection of si-NC cells (Fig. 2b). The colony assay showed that the number of clonogenic spots decreased significantly after the knockdown of RAD51-AS1 (Fig. 2c). Similarly, EdU assays also demonstrated that RAD51-AS1 had a significant impact on hBMSC proliferation. The EdU positivity rate decreased significantly after the knockdown of RAD51-AS1 (Fig. 2d). To further examine whether RAD51-AS1 influenced the proliferation of hBMSCs by affecting cell cycle progression, we performed the flow cytometry analysis. The results showed that the cell cycle progression of hBMSCs after the knockdown of RAD51-AS1 was significantly stalled in the G_1/G_0 phase, with fewer cells in the S-phase compared with the control group (Fig. 2e). The knockdown of RAD51-AS1 caused significant induction of apoptosis in hBMSCs (Fig. 2f) and the TUNEL assay confirmed the same trend (Fig. 2g). However, the osteogenic differentiation was significantly decreased after knocking down RAD51-AS1 expression for 5 days, as demonstrated by the ALP assay (Fig. 2h).

Overexpression RAD51-AS1 Promoted Cell Viability and Osteogenic Differentiation in hBMSCs

To clarify the effects of RAD51-AS1, we constructed an overexpression plasmid to overexpress RAD51-AS1 to achieve exogenous manipulation of RAD51-AS1 expressions in hBMSCs (Fig. 3a). The MTT assays showed that the overexpression of RAD51-AS1 significantly promoted cell viability compared with vector cells (Fig. 3b). The colony assay showed that the number of clonogenic spots increased significantly following the overexpression of RAD51-AS1 (Fig. 3c). Similarly, the EdU assays also demonstrated the significant impact of RAD51-AS1 on hBMSC proliferation. The EdU positivity rate was significantly higher after RAD51-AS1 overexpression (Fig. 3d). Simultaneously, we performed flow cytometry analysis to explore the influence of RAD51-AS1 on the cell cycle progression of hBMSCs.

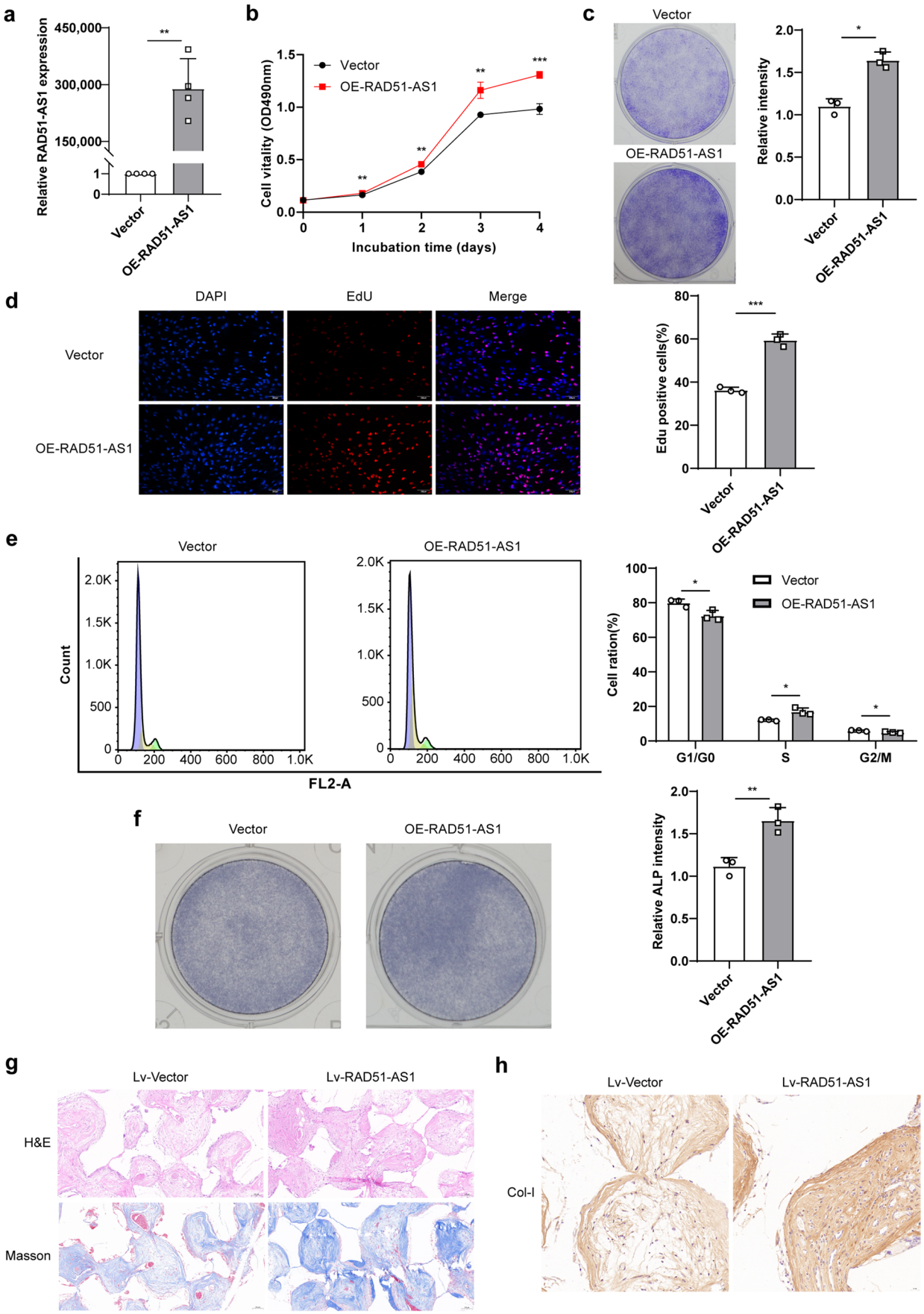
a
Relative RAD51-AS1 expression
450,000
300,000
150,000
1
0
**
Vector
OE-RAD51-AS1
b
Cell vitality (OD490nm)
Vector
OE-RAD51-AS1
Incubation time (days)
c
Vector
OE-RAD51-AS1
Relative intensity
d
DAPI
EdU
Merge
Vector
OE-RAD51-AS1
Edu positive cells(%)
e
Vector
OE-RAD51-AS1
Count
FL2-A
Cell ration(%)
G1/G0
S
G2/M
f
Vector
OE-RAD51-AS1
Relative ALP intensity
g
Lv-Vector
Lv-RAD51-AS1
H&E
Masson
h
Lv-Vector
Lv-RAD51-AS1
Col-I

◂**Fig. 3** Effects on hBMSCs after overexpression of RAD51-AS1. **a** RT-qPCR was used to measure the overexpression efficiency of RAD51-AS1 (n = 4). **b** The MTT assay was performed to determine cell proliferation of hBMSCs after transfection of the overexpression plasmid of RAD51-AS1 (n = 3). **c** The colony formation assay was performed after transfection of overexpression plasmid of RAD51-AS1 to determine the colony-forming ability of transfected hBMSCs (n = 3). **d** The Edu assay was used to detect cell proliferation after transfection of the overexpression plasmid of RAD51-AS1. The positive points were counted and captured (n = 3). **e** At 48 h after transfection of overexpression plasmid of RAD51-AS1, the cell cycle was analyzed by flow cytometry. The bars indicate the percentages of cells in the G1/G0 phase, S phase, or G2/M phase, as shown in the chart (n = 3). **f** ALP staining in the OE-RAD51-AS1 or vector group. **g** Image taken with HE staining and Masson staining of ectopic bone. **h** Image taken with immunohistochemistry of ectopic bone by using the Collagen-I antibody. (The unstained area in the above image is the β-tricalcium phosphate scaffold) *$p < 0.05$, ** $p < 0.01$, and *** $p < 0.001$

The results showed that the cell cycle progression of hBMSCs overexpressing RAD51-AS1 resulted in a significant increase in S-phase progression compared with the vector group (Fig. 3e). After transfection with the RAD51-AS1 plasmid, the osteogenic differentiation was extensively promoted, as determined by ALP assays (Fig. 3f).

Since RAD51-AS1 was mainly expressed in the nucleus, we constructed a lentiviral vector overexpressing RAD51-AS1 and transfected hBMSCs for ectopic osteogenesis assays in vivo. Subsequently, it could be seen from H&E staining, Masson staining, and immunohistochemistry for type I collagen that the overexpression of the RAD51-AS1 group had significantly higher number of osteoblasts and more type I collagen deposition for ectopic bone formation compared to the vector group (Fig. 3g & h).

RAD51-AS1 Functions in hBMSCs by Interacting with the YBX1 Protein

LncRNAs perform biological functions through interactions with transcription factors, histone regulators, and other cellular factors [29]. As we found that RAD51-AS1 is localized in the nucleus, we speculated that RAD51-AS1 interacts with proteins to exert function. To further explore the underlying molecular mechanism, four biotinylated RAD51-AS1 probes and a LacZ probe (negative control) were incubated with total protein extracts from hBMSCs and pulled down with streptavidin (probe sequences are shown in Table S2). ChIRP enriches for human RAD51-AS1. RAD51-AS1 probes retrieved approximately 40-fold higher cellular RAD51-AS1 RNA and undetectable GAPDH compared with the LacZ probe group (Fig. 4a). LacZ probes are used as negative controls and did not retrieve any RNAs. Then, the protein pulled down by ChIRP was analyzed through liquid chromatography coupled with tandem mass spectrometry (LC–MS/MS). In total, 151 proteins were identified in the RAD51-AS1 group and 135 proteins were identified in the LacZ group, among which 68 proteins were RAD51-AS1 specific pull-down proteins (Fig. 4b). Then, we performed the GO enrichment analysis, which showed that the RAD51-AS1-specific pull-down proteins were mainly related to the regulation of the apoptotic signaling pathway and cell aging, which are involved in the progression of osteoporosis (Fig. 4d). We selected proteins with more than two unique peptides from the pull-down proteins for further study (Fig. 4c). We found that YBX1, a DNA- and RBP involved in various disease processes, was of interest among the RAD51-AS1-specific pull-down proteins. It has been reported that YBX1 plays an essential role in tumor progression [30, 31], but the precise role of YBX1 in osteoporosis is still unknown. Consequently, we detected the expression of YBX1 by qPCR and Western blotting. The results showed that the mRNA expression of YBX1 was downregulated after the knockdown of RAD51-AS1 and enhanced after overexpression of RAD51-AS1 (Fig. 4e). Meanwhile, the knockdown of RAD51-AS significantly downregulated the protein level of YBX1. However, the overexpression of RAD51-AS1 upregulated the protein level of YBX1 (Fig. 4f). In addition, the locations of RAD51-AS1 and YBX1 in hBMSCs partly overlapped, providing further indication of the interaction between RAD51-AS1 and YBX1 (Fig. 4g).

RAD51-AS1 Functions in hBMSCs through the TGF-β Signaling Pathway

To further explore the mechanism of the lncRNA RAD51-AS1 in osteoporosis in detail, we constructed a cDNA library by pulling down the polyA tail of the mRNA for RNA sequencing. As shown in the images, the variation in gene expression between the control group and the RAD51-AS1 knockdown group was assessed by heatmap analysis (Fig. 5a) and volcano plot (Fig. 5b). In total, 1099 DE mRNAs were identified between the control and RAD51-AS1 knockdown group, comprising 905 upregulated mRNAs and 194 downregulated mRNAs.

To forecast the function of DE mRNAs, we first analyzed the functions of DE mRNAs via GO, KEGG, and Reactome pathway analyses to provide direction for further study of the mechanism of the lncRNA RAD51-AS1. The Kyoto Encyclopedia of Genes and Genomes (KEGG) pathway analysis revealed that up- and down-regulated mRNAs were mainly involved in the TGF-β signaling pathway, the Wnt signaling pathway, and apoptosis (Fig. 5c). Gene set enrichment analysis (GSEA) revealed that the gene sets were significantly related to the TGF-β pathway (Fig. 5d). The significant enrichment was shown by GO analysis identified up- and down-regulation mRNAs that primarily participated in skeletal system development (Fig. 5e).

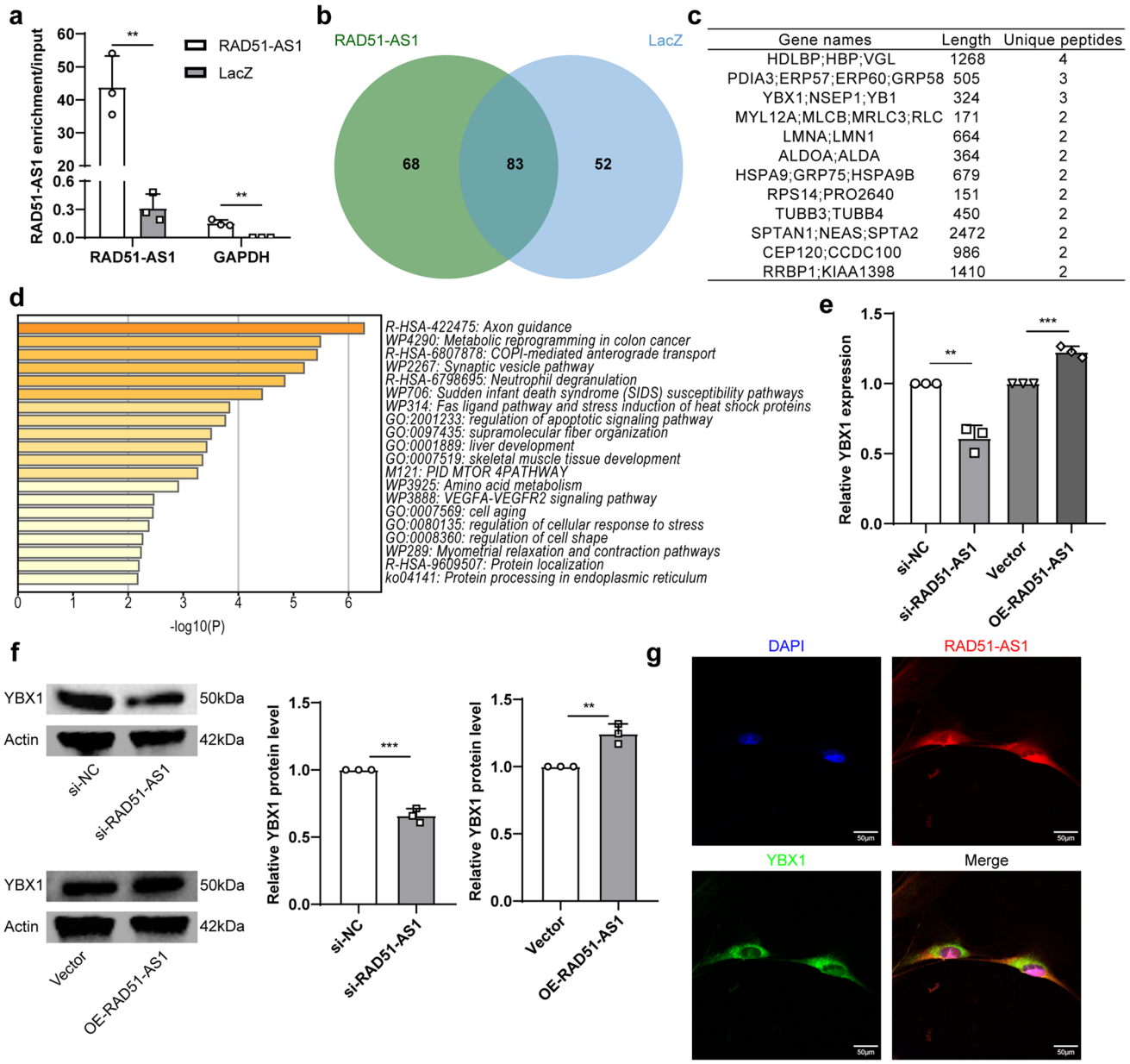

Gene names	Length	Unique peptides
HDLBP;HBP;VGL	1268	4
PDIA3;ERP57;ERP60;GRP58	505	3
YBX1;NSEP1;YB1	324	3
MYL12A;MLCB;MRLC3;RLC	171	2
LMNA;LMN1	664	2
ALDOA;ALDA	364	2
HSPA9;GRP75;HSPA9B	679	2
RPS14;PRO2640	151	2
TUBB3;TUBB4	450	2
SPTAN1;NEAS;SPTA2	2472	2
CEP120;CCDC100	986	2
RRBP1;KIAA1398	1410	2

Fig. 4 Identifying RBPs that interact with RAD51-AS1. **a** CHIRP assay analysis using four Biotin-TEG-labeled probes for RAD51-AS1 showed that RAD51-AS1 probes retrieve about 40-fold more cellular RAD51-AS1 RNA and undetectable GAPDH compared with hBMSCs when LacZ was used as the negative control (n = 3). **b** Venn diagram depicting the number of repressed genes identified in the RAD51-AS1 and LacZ group. **c** Proteins pulled down with RAD51-AS1 and LacZ probes that are only pulled down specifically by RAD51-AS1 and have a specific peptide segment of > 2. **d** Gene ontology analysis for all proteins pulled down with the four Biotin-TEG-labeled probes for RAD51-AS1. **e** The RT-qPCR and western blotting assays detected the expression of YBX1 after knockdown or overexpression of RAD51-AS1 (n = 3). **f** The western blotting assays detected the expression of YBX1 after knockdown or overexpression of RAD51-AS1 (n = 3). **g** RAD51-AS1 RNA FISH was performed in hBMSCs and showed that RAD51-AS1 could partly colocalize with YBX1 (n = 3). *p < 0.05, ** p < 0.01, and *** p < 0.001

After we verified the expression of RNA-seq by qPCR, we confirmed that CDKN2B, CEBPA, CSF1R, DDIT3, ID2, ID4, SMAD7, and SMURF2 were upregulated in the RAD51-AS1 knockdown group, whereas PCNA, SIVA1, and ZYX were downregulated (Fig. 5f).

Perturbations in the TGF-β pathways are associated with numerous human diseases, with prominent involvement of the skeletal systems via the stimulation of bone formation [32]. Moreover, we speculate that the TGF-β signaling pathway plays a key role in osteoporosis progression via the lncRNA RAD51-AS1, as shown through the RNA-seq and

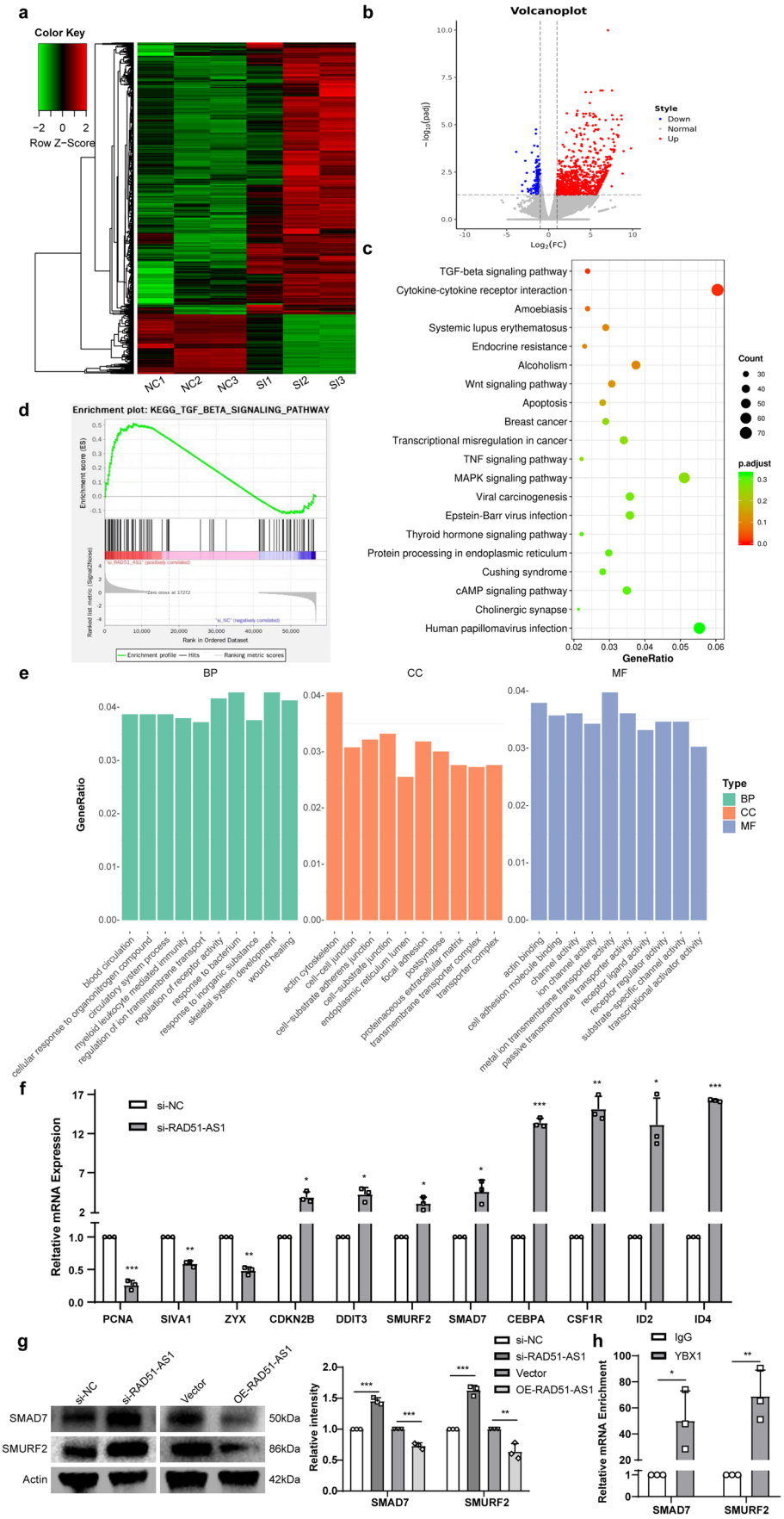

Fig. 5 Mechanism of RAD51-AS1 affecting TGF-β pathway through YBX1. **a** Heatmap depicting differentially expressed genes between si-NC and si-RAD51-AS1 treatments. **b** The volcano plot shows the differentially expressed genes with the cutoff fold-changes of ≥ 1 or ≤ -1 and FDR < 0.05. **c** The gene ontology analysis for all genes with altered expression after knockdown of RAD51-AS1. **d** The GSEA showed that genes in response to RAD51-AS1 knockdown are enriched for the gene sets significantly related to the TGF-β pathway. **e** The KEGG analysis for all genes with altered expression after knockdown of RAD51-AS1. **f** The altered mRNA levels of genes were selectively confirmed by qRT-PCR in knockdown RAD51-AS1 (n = 3). **g** The western blotting assays detected the expression of SMAD7 and SMURF2 after knockdown or overexpression of RAD51-AS1 (n = 3). **h** RIP experiments using anti-YBX1 were performed, and the coprecipitated RNA was analyzed by qRT-PCR to examine the expression of SMAD7 and SMURF2. The fold enrichment of mRNAs in RIP was relative to its matching IgG control RIP (n = 3). *p < 0.05, ** p < 0.01, and *** p < 0.001

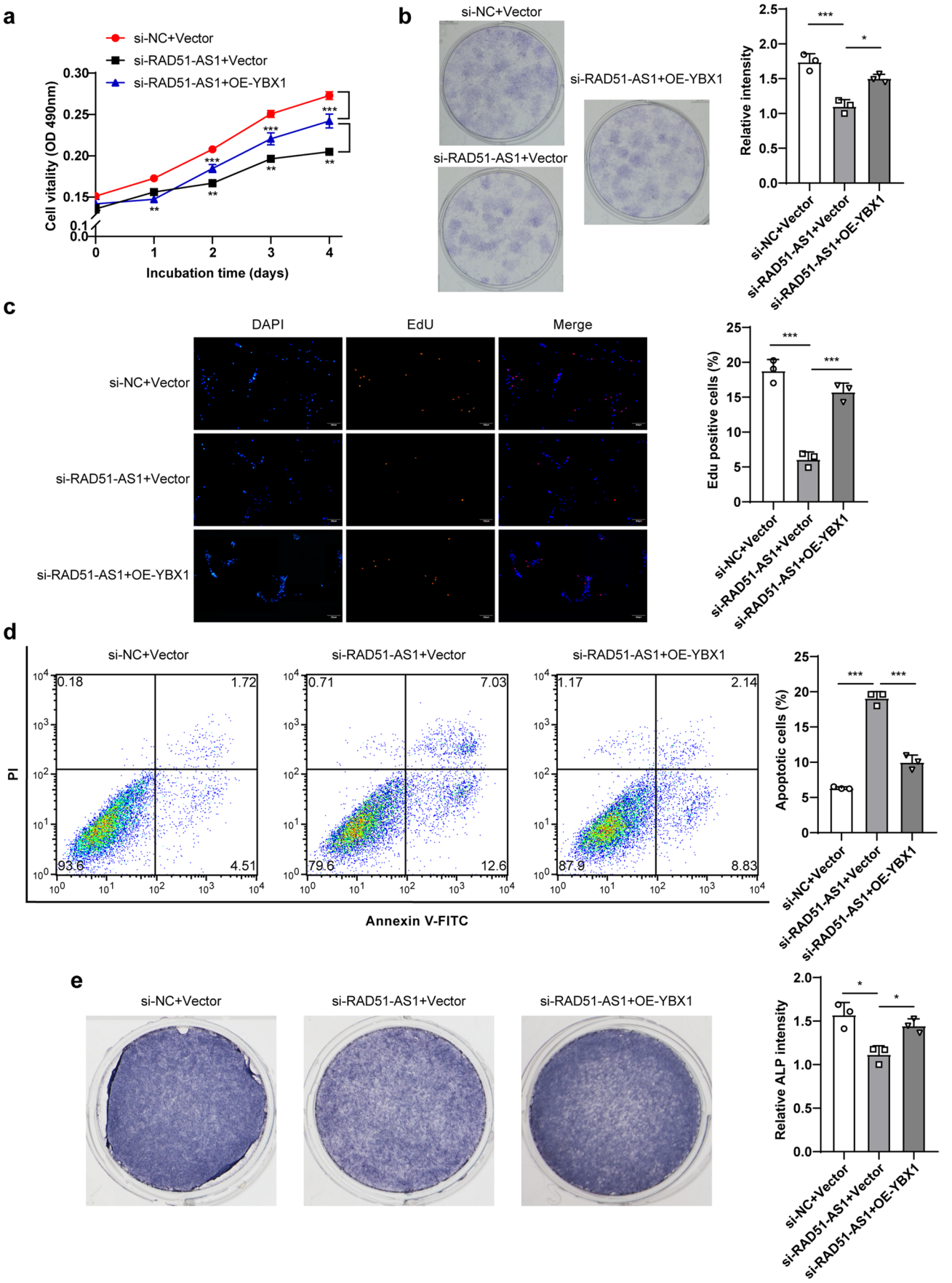
a
si-NC+Vector
si-RAD51-AS1+Vector
si-RAD51-AS1+OE-YBX1
Cell vitality (OD 490nm)
Incubation time (days)
b
si-NC+Vector
si-RAD51-AS1+Vector
si-RAD51-AS1+OE-YBX1
Relative intensity
c
DAPI
EdU
Merge
si-NC+Vector
si-RAD51-AS1+Vector
si-RAD51-AS1+OE-YBX1
Edu positive cells (%)
d
si-NC+Vector
si-RAD51-AS1+Vector
si-RAD51-AS1+OE-YBX1
PI
Annexin V-FITC
0.18
1.72
93.6
4.51
0.71
7.03
79.6
12.6
1.17
2.14
87.9
8.83
Apoptotic cells (%)
e
si-NC+Vector
si-RAD51-AS1+Vector
si-RAD51-AS1+OE-YBX1
Relative ALP intensity

◂**Fig. 6** Demonstrating that RAD51-AS1 plays a role in ameliorating osteoporosis via YBX1. **a** The MTT assay was used to detect cell proliferation after RAD51-AS1 knockdown in hBMSCs transfected with the overexpression plasmid of YBX1 (n = 3). **b** The colony formation assay was used to detect the colony-forming capacity of hBSMCs transfected with the overexpression plasmid of YBX1 after RAD51-AS1 knockdown (n = 3). **c** The EdU assay was used to determine the cell proliferation after RAD51-AS1 knockdown in hBSMCs transfected with the overexpression plasmid of YBX1 (n = 3). **d** At 48 h after RAD51-AS1 knockdown in hBSMCs transfected with the overexpression plasmid of YBX1, hBMSCs were stained and analyzed by flow cytometry. Apoptotic cells include early and terminal apoptotic cells (n = 3). **e** The ALP staining in the si-RAD51-AS1 with the overexpression plasmid of YBX1, si-RAD51-AS1, and si-NC groups (n = 3). *p < 0.05, ** p < 0.01, and *** p < 0.001

functional enrichment analyses. Besides, forming a complex of mRNA with YBX1 to repress the translation of SMAD7 and SUMRF2 is a key way to affect the TGF-β pathway [33]. SMURF2 not only binds SMAD7 to form an E3 ubiquitin ligase that targets the TGFβ receptor for degradation to repress the TGF-β pathway [34] but also negatively regulates the TGF-β/BMP signaling pathway through ubiquitination [35]. Then, we performed Western blotting, and the results suggested that SMAD7 and SMURF2 protein levels were significantly increased after knocking down RAD51-AS1. However, the overexpression of RAD51-AS1 resulted in the opposite trend effect on hBMSCs (Fig. 5g). In addition, the RIP assay demonstrated that YBX1 could pull down the mRNA of SMAD7 and SMURF2 in hBMSCs (Fig. 5h).

RAD51-AS1 Regulates hBMSC Osteogenesis and Apoptosis via Binding to YBX1

To determine if RAD51-AS1 functions by binding YBX1, we overexpressed YBX1 after knocking down RAD51-AS1 to perform the subsequent experiments. The results of the MTT assays showed that the overexpression of YBX1 partially rescued the reduction in hBMSC proliferation and colony formation efficacy induced by the knockdown of RAD51-AS1 (Fig. 6a & b). The EdU assays also demonstrated that the EdU positivity rate was lowest after the knockdown of RAD51-AS1, whereas the overexpression of YBX1 significantly increased the EdU positivity rate in hBMSCs after RAD51-AS1 knockdown (Fig. 6c). Moreover, the percentages of apoptotic hBMSCs were dramatically decreased by overexpression of YBX1 in hBMSCs after RAD51-AS1 knockdown but were not decreased to control levels (Fig. 6d). In contrast, osteogenic ALP-positive areas were increased significantly by overexpressing YBX1 in hBMSCs after RAD51-AS1 knockdown (Fig. 6e).

RAD51-AS1 Binds to YBX1 to Regulate the Promoter of Downstream Target Genes

Previous experiments have shown that YBX1 can function as a transcription factor and that RAD51-AS1 mainly functions in the nuclei. Thus, we performed CUT&Tag assays to investigate the binding sites of YBX1 on DNA to identify the downstream genes in combination with the mRNA-seq results. We then used the YBX1 antibody to pull down the bound DNA from hBSMCs to build a library for next-generation gene sequencing. The heatmap of all YBX1 signals, normalized by RPKM to the genomic region controlled by CUT&Tag IgG, revealed that YBX1 was mainly enriched in the TSS region of the genome (Fig. 7a) and that the peak enrichment is centered on the TSS, to the positive and negative expansion distance of 2 k (Fig. 7b). We then used the UCSC genome browser (http://genome-asia.ucsc.edu/) in combination with differentially expressed genes in RNA-seq to identify the target genes: PCNA and SIVA1. The peaks of YBX1 demonstrated that YBX1 was capable of binding to the promoter regions of PCNA and SIVA1 (Fig. 7c).

To demonstrate the function of RAD51-AS1 and YBX1 complexes, we used hBMSCs treated with the si-NC or si-RAD51-AS1 to perform the CUT&Tag assays. We also designed three specific SIVA1 promoter primers and one specific PCNA promoter primer. The qPCR results revealed that the knockdown of RAD51-AS1 could affect the binding with YBX1 in the promoter region of the target genes, especially in the P2 fragment of SIVA1 (Fig. 7d). In the meantime, the mRNA expression of PCNA and SIVA1 also decreased after silencing the expression of RAD51-AS1 by qPCR (Fig. 5f).

In conclusion, RAD51-AS1 ameliorates osteoporosis by binding to YBX1, which inhibits the translation of SMAD7 and SMURF2 and transcriptional up-regulated PCNA and SIVA1.

Discussion

BMSCs have the ability to differentiate into multiple cell types, including osteogenic, chondrogenic and adipogenic lineages [36]. Inducing BMSC osteogenesis represents a potential treatment that promotes bone formation and bone regeneration. With the recent extensive study of lncRNAs, an increasing number of lncRNAs are being studied in the BMSC field. Furthermore, some lncRNAs have been confirmed to regulate BMSC osteogenesis [37]. Therefore, exploring new target genes and therapeutic methods for osteoporosis is essential. Herein, we selected RAD51-AS1 to study whether it is a protective target against osteoporosis by stimulating the proliferation and osteogenic differentiation of

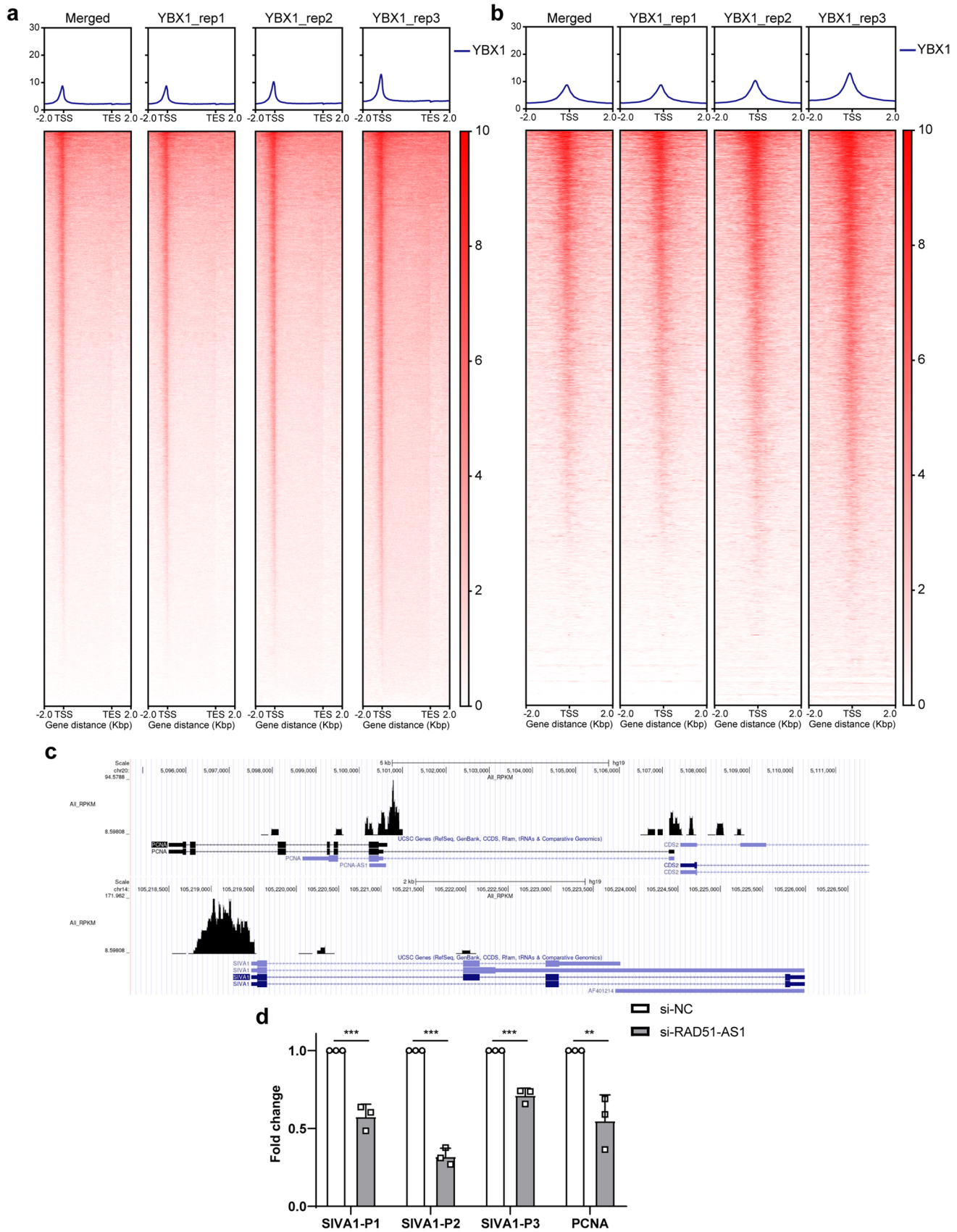
a
Merged
YBX1_rep1
YBX1_rep2
YBX1_rep3
YBX1
-2.0 TSS
TES 2.0
Gene distance (Kbp)
b
Merged
YBX1_rep1
YBX1_rep2
YBX1_rep3
YBX1
-2.0
TSS
2.0
Gene distance (Kbp)
c
All_RPKM
UCSC Genes (RefSeq, GenBank, CCDS, Rfam, tRNAs & Comparative Genomics)
PCNA
PCNA-AS1
SIVA1
AF401214
d
si-NC
si-RAD51-AS1
Fold change
SIVA1-P1
SIVA1-P2
SIVA1-P3
PCNA

◂**Fig. 7** RAD51-AS1 affects the transcriptional regulation of target genes via YBX1. **a, b** Heatmaps of binding site patterns of YBX1 detected by the CUT&Tag assay in hBSMCs from three experimental repeats. TSS, transcription start site; TES, transcription end site (n = 3). **c** UCSC views of the sequencing data at YBX1 target loci normalized by RPKM to the genomic region controlled by CUT&Tag IgG. **d** CUT-Tag-qPCR of YBX1 of these gene loci promoter regions after knockdown RAD51-AS1 in hBMSCs. Antibody enrichment was quantified relative to the amount of input DNA (n = 3)

hBMSCs. We reannotated the GSE35956 datasets, compared and analyzed the differential expression profiles of lncRNAs between hBMSCs from healthy and osteoporotic patients, and then screened a lncRNA RAD51-AS1 with low expression in hBMSCs from osteoporotic patients and confirmed that the expression level of lncRNA RAD51-AS1 in hBMSCs from patients with osteoporosis was significantly lower than these from healthy donors using real-time RT-PCR. LncRNA RAD51-AS1 increased viability and osteogenic differentiation but reduced apoptosis of hBMSCs. Mechanistically, RAD51-AS1 could bind specifically to YBX1 to perform a protective role in hBSMCs. Considering all of the above findings, we concluded that RAD51-AS1 is a vital molecule in hBMSCs, emphasizing its novel in the pathogenesis of osteoporosis.

LncRNAs modulate various aspects of the function of BMSCs and thus influence the process of osteoporosis [38]. The presence of lncRNA RAD51-AS1 has been reported in tumors, including colorectal cancer, epithelial ovarian cancer, hepatocellular carcinoma, and breast cancer. An abnormal elevation of RAD51-AS1 can reduce p53 expression in epithelial ovarian cancer [39]. However, lncRNA RAD51-AS1 repressed colorectal cancer, inhibiting proliferation, invasion, and glycolysis via the miR-29b/c-3p/NDRG2 axis [40]. Moreover, lncRNA RAD51-AS1 binds to RAD51 mRNA and downregulates the RAD51 protein in hepatocellular carcinoma [41, 42]. Another study indicated that lncRNA RAD51-AS1 could enhance RAD51-dependent DNA repair capacity in breast cancer cells [43]. However, the role and mechanism of osteoporosis have not yet been reported. In our current research, the results revealed that RAD51-AS1 played a vital role in protecting against the progression of osteoporosis by stimulating the proliferation and osteogenic differentiation of hBMSCs and inhibiting their apoptosis. In vivo ectopic bone formation assays provided stronger evidence that RAD51-AS1 increases type I collagen expression and collagen fiber production, thereby promoting new bone formation.

The subcellular fates of lncRNAs are distinct, and their mechanisms of action are diverse. Therefore, clarifying the cellular sub-localization of RAD51-AS1 is particularly important to determine how it exerts its effect [44, 45]. From the nucleoplasmic separation and RNA-FISH experiments, we demonstrated that RAD51-AS1 is mainly located in the nucleus of hBMSCs. It has been reported that nuclear lncRNAs are enriched for functionality involving chromatin interactions, transcriptional regulation, and RNA processing [46]. The ChIRP assays and mass spectrometry results showed that YBX1 specifically bound the most peptides among the pulled-down RBPs. YBX1 was identified as a DNA/RNA-binding protein, and is involved in oncogenic cell transformation, multiple drug resistance, and dissemination of tumors [33, 47]. Further evidence showed that YBX1 could bind to mRNAs that predominantly belong to the groups related to proliferation, differentiation, or binding of nucleic acids via high-throughput experiments [48]. However, the role of YBX1 in osteoporosis has not yet been reported.

Interestingly, YBX1 can also concurrently bind mRNA to repress protein translation by packing mRNA with YBX1 [49, 50]. First, we found that RAD51-AS1 exerts its function in hBMSCs mainly through the TGF-β signaling pathway. In the meanwhile, RAD51-AS1 in hBSMCs was shown to affect the expression of SMAD7, SMURF2, and YBX1. Moreover, the RIP assay demonstrated that YBX1 could bind with the mRNA of SMAD7 and SMURF2. According to previous reports, SMAD7 and SMURF2 can cause the degradation of TGFBR1 through multiple pathways [51]. For example, Smad7 regulates the function of Smurf2 and promotes the degradation of type I receptors by recruiting UbcH7 to the HECT structural domain [52]; SIK interacts and cooperates with the Smad7-Smurf2 complex to promote the downregulation of activated TβRI receptors [53], and Smad7 binds to Smurf2 to form an E3 ubiquitin ligase that targets TGF β receptors for degradation [34]. Meanwhile, TGF-β can promote cell proliferation and osteogenic differentiation of BMSCs under certain conditions [54, 55]. Thus, we speculated that RAD51-AS1 affected the TGF-β pathway by SMAD7 and SMURF2, which could form an mRNA–protein complex with YBX1 to repress the translation of SMAD7 and SMURF2.

In addition, YBX1 is a characterized transcription factor regulating the promoter activity of target genes. YBX1 specifically enhances the transcriptional regulation of PCNA and SIVA1 as demonstrated by CUT&Tag assay and qPCR. As we know, proliferating cell nuclear antigen (PCNA) is regarded as a critical gene that promotes BMSC proliferation [56]. In addition, Siva1 mainly inhibits p53 function by acting as an ARF E3 ubiquitin ligase or a necessary adaptor promoting degradation through Hdm2 [57, 58]. Moreover, p53 activity can influence the cell fate specification and osteogenic differentiation of BMSCs as a negative regulator [59, 60]. In this study, we found that RAD51-AS1 can also bind the promoter region of PCNA and SIVA1 by interacting with YBX1, which enhances their transcription.

However, the progression of osteoporosis is a complex process in which various aspects are involved. So, we can

further compare the expression of RAD51-AS1 between bone tissues from normal people and osteoporosis patients. In the present work, our experiments were mainly based on hBMSCs, and we still need to demonstrate its protective effect against osteoporosis by constructing RAD51-AS1 knockout mice or conditional knockout mice in the future. Further studies on the role and mechanism of the SIVA1 gene in osteoporosis may also better explain the role of RAD51-AS1.

In conclusion, our findings indicate that RAD51-AS1 stimulated the osteogenesis of hBMSCs by binding to YBX1, then inhibiting the translation of SMAD7 and SMURF2 by binding with their mRNA and transcriptionally up-regulated PCNA and SIVA1 by binding with their promoter regions. Therefore, we suggest that RAD51-AS1 may be a target for protection against osteoporosis by stimulating the proliferation and osteogenic differentiation of hBMSCs.

Abbreviations BMSCs: Bone marrow mesenchymal stem cells; hBMSCs: Human Bone marrow mesenchymal stem cells; LncRNAs: Long noncoding RNAs; RBP: RNA-binding protein; ALP: Alkaline phosphatase; FISH: Fluorescent in situ hybridization; IF: Immunofluorescence; CHIRP: Chromatin isolation by RNA purification; RIP: RNA immunoprecipitation; CUT&Tag: Cleavage under targets and tagmentation; SD: Standard deviation; ANOVA: Analysis of variance

Supplementary Information The online version contains supplementary material available at https://doi.org/10.1007/s12015-022-10408-x.

Acknowledgements We thank Prof. Deng-Shun Miao for the research platform and our partners in A426 lab for their help. We also thank HaploX for providing bioinformatics analysis.

Authors' Contributions Qiang Sun, Dengshun Miao, and Beichen Li were involved in the conception and design of this study. Beichen Li performed the experiments and wrote the manuscript. Jing Wang and Fangrong Xu provided suggestions and performed the analysis. Qinjue Wang provided suggestions for revisions and embellished the article. Liu Quan and Wang Guan Tong insightfully discussed and revised the manuscript. All authors read and approved the final submitted manuscript.

Funding This work was supported by the National Natural Science Foundation of China (Grant No. 81730066) and the Nanjing Health Science and Technology Development Special Funds (Grant No. ZKX19025).

Data Availability GSE35956 raw data were downloaded from The Gene Expression Omnibus (GEO) database (https://www.ncbi.nlm.nih.gov/geo/query/acc.cgi?acc=GSE35956).

Declarations

Ethics Approval and Consent to Participate This study was approved by the ethics committee of the Nanjing First Hospital Medical University (approval number: 00001501). Written informed consent was obtained from all participants included in the study.

This study was performed in strict accordance with the recommendations in the Guide for the Care and Use of Laboratory Animals of the Nanjing Medical University. All procedures involving animals were approved by the Animal Use and Care Committee of the Nanjing Medical University (approval number: IACUC-2203058).

Consent for Publication Not applicable.

The datasets supporting the conclusions of this article are included within the article.

Competing Interests The authors declare no competing interests.

References

1. Florencio-Silva, R., Sasso, G. R., Sasso-Cerri, E., Simoes, M. J., & Cerri, P. S. (2015). Biology of Bone Tissue: Structure, Function, and Factors That Influence Bone Cells. *BioMed Research International, 2015*, 421746.
2. Yang, T. L., Shen, H., Liu, A., Dong, S. S., Zhang, L., Deng, F. Y., et al. (2020). A road map for understanding molecular and genetic determinants of osteoporosis. *Nature Reviews Endocrinology, 16*, 91–103.
3. Rachner, T. D., Khosla, S., & Hofbauer, L. C. (2011). Osteoporosis: Now and the future. *Lancet, 377*, 1276–1287.
4. Burge, R., Dawson-Hughes, B., Solomon, D. H., Wong, J. B., King, A., & Tosteson, A. (2007). Incidence and economic burden of osteoporosis-related fractures in the United States, 2005–2025. *Journal of Bone and Mineral Research, 22*, 465–475.
5. Compston, J. E., McClung, M. R., & Leslie, W. D. (2019). *Osteoporosis. Lancet., 393*, 364–376.
6. Lizneva, D., Yuen, T., Sun, L., Kim, S. M., Atabiekov, I., Munshi, L. B., et al. (2018). Emerging concepts in the epidemiology, pathophysiology, and clinical care of osteoporosis across the menopausal transition. *Matrix Biology, 71–72*, 70–81.
7. Bianco, P., Robey, P. G., & Simmons, P. J. (2008). Mesenchymal stem cells: Revisiting history, concepts, and assays. *Cell Stem Cell, 2*, 313–319.
8. de Paula, F. J. A., & Rosen, C. J. (2020). Marrow Adipocytes: Origin, Structure, and Function. *Annual Review of Physiology, 82*, 461–484.
9. Grayson, W. L., Bunnell, B. A., Martin, E., Frazier, T., Hung, B. P., & Gimble, J. M. (2015). Stromal cells and stem cells in clinical bone regeneration. *Nature Reviews. Endocrinology, 11*, 140–150.
10. Sacchetti, B., Funari, A., Michienzi, S., Di Cesare, S., Piersanti, S., Saggio, I., et al. (2007). Self-renewing osteoprogenitors in bone marrow sinusoids can organize a hematopoietic microenvironment. *Cell, 131*, 324–336.
11. Infante, A., & Rodriguez, C. I. (2018). Osteogenesis and aging: Lessons from mesenchymal stem cells. *Stem Cell Research & Therapy, 9*, 244.
12. Li, H., Liu, P., Xu, S., Li, Y., Dekker, J. D., Li, B., et al. (2017). FOXP1 controls mesenchymal stem cell commitment and senescence during skeletal aging. *The Journal of Clinical Investigation, 127*, 1241–1253.
13. Moerman, E. J., Teng, K., Lipschitz, D. A., & Lecka-Czernik, B. (2004). Aging activates adipogenic and suppresses osteogenic programs in mesenchymal marrow stroma/stem cells: The role of PPAR-gamma2 transcription factor and TGF-beta/BMP signaling pathways. *Aging Cell, 3*, 379–389.
14. Wang, Y., Deng, P., Liu, Y., Wu, Y., Chen, Y., Guo, Y., et al. (2020). Alpha-ketoglutarate ameliorates age-related osteoporosis via regulating histone methylations. *Nature Communications, 11*, 5596.

15. Zheng J, Guo H, Qin Y, Liu Z, Ding Z, Zhang L, et al. (2020). SNHG5/miR-582–5p/RUNX3 feedback loop regulates osteogenic differentiation and apoptosis of bone marrow mesenchymal stem cells. *Journal of Cellular Physiology*.
16. Carninci, P., Kasukawa, T., Katayama, S., Gough, J., Frith, M. C., Maeda, N., et al. (2005). The transcriptional landscape of the mammalian genome. *Science, 309*, 1559–1563.
17. Ng, S. Y., Johnson, R., & Stanton, L. W. (2012). Human long noncoding RNAs promote pluripotency and neuronal differentiation by association with chromatin modifiers and transcription factors. *EMBO Journal, 31*, 522–533.
18. Sun, L., Goff, L. A., Trapnell, C., Alexander, R., Lo, K. A., Hacisuleyman, E., et al. (2013). Long noncoding RNAs regulate adipogenesis. *Proc Natl Acad Sci U S A., 110*, 3387–3392.
19. Wang, K. C., & Chang, H. Y. (2011). Molecular mechanisms of long noncoding RNAs. *Molecular Cell, 43*, 904–914.
20. Tsai, M. C., Manor, O., Wan, Y., Mosammaparast, N., Wang, J. K., Lan, F., et al. (2010). Long noncoding RNA as modular scaffold of histone modification complexes. *Science, 329*, 689–693.
21. Xu, F., Li, W., Yang, X., Na, L., Chen, L., & Liu, G. (2020). The Roles of Epigenetics Regulation in Bone Metabolism and Osteoporosis. *Front Cell Dev Biol., 8*, 619301.
22. Li, C. J., Xiao, Y., Yang, M., Su, T., Sun, X., Guo, Q., et al. (2018). Long noncoding RNA Bmncr regulates mesenchymal stem cell fate during skeletal aging. *The Journal of Clinical Investigation, 128*, 5251–5266.
23. Jin, F., Li, J., Zhang, Y. B., Liu, X., Cai, M., Liu, M., et al. (2021). A functional motif of long noncoding RNA Nron against osteoporosis. *Nature Communications, 12*, 3319.
24. Li, M., Xie, Z., Li, J., Lin, J., Zheng, G., Liu, W., et al. (2020). GAS5 protects against osteoporosis by targeting UPF1/SMAD7 axis in osteoblast differentiation. *Elife*, *9*.
25. Zhang, X., Sun, S., Pu, J. K., Tsang, A. C., Lee, D., Man, V. O., et al. (2012). Long non-coding RNA expression profiles predict clinical phenotypes in glioma. *Neurobiology of Diseases, 48*, 1–8.
26. Su, X., Wang, H., Ge, W., Yang, M., Hou, J., Chen, T., et al. (2015). An In Vivo Method to Identify microRNA Targets Not Predicted by Computation Algorithms: P21 Targeting by miR-92a in Cancer. *Cancer Research, 75*, 2875–2885.
27. Lv, F. J., Tuan, R. S., Cheung, K. M., & Leung, V. Y. (2014). Concise review: The surface markers and identity of human mesenchymal stem cells. *Stem Cells., 32*, 1408–1419.
28. Li, H., Ghazanfari, R., Zacharaki, D., Lim, H. C., & Scheding, S. (2016). Isolation and characterization of primary bone marrow mesenchymal stromal cells. *Annals of the New York Academy of Sciences, 1370*, 109–118.
29. Yao, R. W., Wang, Y., & Chen, L. L. (2019). Cellular functions of long noncoding RNAs. *Nature Cell Biology, 21*, 542–551.
30. Chen, Q., Wang, H., Li, Z., Li, F., Liang, L., Zou, Y., et al. (2022). Circular RNA ACTN4 promotes intrahepatic cholangiocarcinoma progression by recruiting YBX1 to initiate FZD7 transcription. *Journal of Hepatology, 76*, 135–147.
31. Feng, M., Xie, X., Han, G., Zhang, T., Li, Y., Li, Y., et al. (2021). YBX1 is required for maintaining myeloid leukemia cell survival by regulating BCL2 stability in an m6A-dependent manner. *Blood, 138*, 71–85.
32. MacFarlane, E. G., Haupt, J., Dietz, H. C., Shore, E. M. (2017). TGF-beta Family Signaling in Connective Tissue and Skeletal Diseases. *Cold Spring Harbor Perspectives in Biology*, *9*.
33. Mordovkina D, Lyabin DN, Smolin EA, Sogorina EM, Ovchinnikov LP, Eliseeva I. Y-Box Binding Proteins in mRNP Assembly, Translation, and Stability Control. Biomolecules. 2020; 10.
34. Kavsak, P., Rasmussen, R. K., Causing, C. G., Bonni, S., Zhu, H., Thomsen, G. H., et al. (2000). Smad7 binds to Smurf2 to form an E3 ubiquitin ligase that targets the TGF beta receptor for degradation. *Molecular Cell, 6*, 1365–1375.
35. Kushioka, J., Kaito, T., Okada, R., Ishiguro, H., Bal, Z., Kodama, J., et al. (2020). A novel negative regulatory mechanism of Smurf2 in BMP/Smad signaling in bone. *Bone Res., 8*, 41.
36. Caplan, A. I., & Bruder, S. P. (2001). Mesenchymal stem cells: Building blocks for molecular medicine in the 21st century. *Trends in Molecular Medicine, 7*, 259–264.
37. Ju, C., Liu, R., Zhang, Y. W., Zhang, Y., Zhou, R., Sun, J., et al. (2019). Mesenchymal stem cell-associated lncRNA in osteogenic differentiation. *Biomedicine & Pharmacotherapy, 115*, 108912.
38. Xie, Z. Y., Wang, P., Wu, Y. F., & Shen, H. Y. (2019). Long noncoding RNA: The functional regulator of mesenchymal stem cells. *World J Stem Cells., 11*, 167–179.
39. Zhang, X., Liu, G., Qiu, J., Zhang, N., Ding, J., & Hua, K. (2017). E2F1-regulated long non-coding RNA RAD51-AS1 promotes cell cycle progression, inhibits apoptosis and predicts poor prognosis in epithelial ovarian cancer. *Science and Reports, 7*, 4469.
40. Li, C., Wang, P., Du, J., Chen, J., Liu, W., & Ye, K. (2021). LncRNA RAD51-AS1/miR-29b/c-3p/NDRG2 crosstalk repressed proliferation, invasion and glycolysis of colorectal cancer. *IUBMB Life, 73*, 286–298.
41. Chen, C. C., Chen, C. Y., Ueng, S. H., Hsueh, C., Yeh, C. T., Ho, J. Y., et al. (2018). Corylin increases the sensitivity of hepatocellular carcinoma cells to chemotherapy through long noncoding RNA RAD51-AS1-mediated inhibition of DNA repair. *Cell Death & Disease, 9*, 543.
42. Chen, C. C., Chen, C. Y., Wang, S. H., Yeh, C. T., Su, S. C., Ueng, S. H., et al. (2018). Melatonin sensitizes hepatocellular carcinoma cells to chemotherapy through long non-coding RNA RAD51-AS1-mediated suppression of DNA repair. Cancers (Basel). 10.
43. Gazy, I., Zeevi, D. A., Renbaum, P., Zeligson, S., Eini, L., Bashari, D., et al. (2015). TODRA, a lncRNA at the RAD51 locus, is oppositely regulated to RAD51, and enhances RAD51-dependent DSB (double strand break) repair. *PLoS ONE, 10*, e0134120.
44. Bridges, M. C., Daulagala, A. C., Kourtidis, A. (2021). LNCcation: lncRNA localization and function. *Journal of Cell Biology*, *220*.
45. Chen, L. L. (2016). Linking Long Noncoding RNA Localization and Function. *Trends in Biochemical Sciences, 41*, 761–772.
46. Schmitt, A. M., & Chang, H. Y. (2016). Long Noncoding RNAs in Cancer Pathways. *Cancer Cell, 29*, 452–463.
47. Kwon, E., Todorova, K., Wang, J., Horos, R., Lee, K. K., Neel, V. A., et al. (2018). The RNA-binding protein YBX1 regulates epidermal progenitors at a posttranscriptional level. *Nature Communications, 9*, 1734.
48. Evdokimova, V., Tognon, C., Ng, T., Ruzanov, P., Melnyk, N., Fink, D., et al. (2009). Translational activation of snail1 and other developmentally regulated transcription factors by YB-1 promotes an epithelial-mesenchymal transition. *Cancer Cell, 15*, 402–415.
49. Evdokimova, V., Ovchinnikov, L. P., & Sorensen, P. H. (2006). Y-box binding protein 1: Providing a new angle on translational regulation. *Cell Cycle, 5*, 1143–1147.
50. Kretov, D. A., Curmi, P. A., Hamon, L., Abrakhi, S., Desforges, B., Ovchinnikov, L. P., et al. (2015). mRNA and DNA selection via protein multimerization: YB-1 as a case study. *Nucleic Acids Research, 43*, 9457–9473.
51. Miyazawa, K., Miyazono, K. (2017). Regulation of TGF-beta Family Signaling by Inhibitory Smads. *Cold Spring Harbor Perspectives in Biology*, *9*.
52. Ogunjimi, A. A., Briant, D. J., Pece-Barbara, N., Le Roy, C., Di Guglielmo, G. M., Kavsak, P., et al. (2005). Regulation of Smurf2 ubiquitin ligase activity by anchoring the E2 to the HECT domain. *Molecular Cell, 19*, 297–308.

53. Kowanetz, M., Lonn, P., Vanlandewijck, M., Kowanetz, K., Heldin, C. H., & Moustakas, A. (2008). TGFbeta induces SIK to negatively regulate type I receptor kinase signaling. *Journal of Cell Biology, 182*, 655–662.
54. Maeda, S., Hayashi, M., Komiya, S., Imamura, T., & Miyazono, K. (2004). Endogenous TGF-beta signaling suppresses maturation of osteoblastic mesenchymal cells. *EMBO Journal, 23*, 552–563.
55. Ng, F., Boucher, S., Koh, S., Sastry, K. S., Chase, L., Lakshmipathy, U., et al. (2008). PDGF, TGF-beta, and FGF signaling is important for differentiation and growth of mesenchymal stem cells (MSCs): Transcriptional profiling can identify markers and signaling pathways important in differentiation of MSCs into adipogenic, chondrogenic, and osteogenic lineages. *Blood, 112*, 295–307.
56. Lei, Q., Gao, F., Liu, T., Ren, W., Chen, L., Cao, Y., et al. (2021). Extracellular vesicles deposit PCNA to rejuvenate aged bone marrow-derived mesenchymal stem cells and slow age-related degeneration. *Science Translational Medicine*, *13*.
57. Du, W., Jiang, P., Li, N., Mei, Y., Wang, X., Wen, L., et al. (2009). Suppression of p53 activity by Siva1. *Cell Death and Differentiation, 16*, 1493–1504.
58. Wang, X., Zha, M., Zhao, X., Jiang, P., Du, W., Tam, A. Y., et al. (2013). Siva1 inhibits p53 function by acting as an ARF E3 ubiquitin ligase. *Nature Communications, 4*, 1551.
59. Wang, X., Kua, H. Y., Hu, Y., Guo, K., Zeng, Q., Wu, Q., et al. (2006). p53 functions as a negative regulator of osteoblastogenesis, osteoblast-dependent osteoclastogenesis, and bone remodeling. *Journal of Cell Biology, 172*, 115–125.
60. He, Y., de Castro, L. F., Shin, M. H., Dubois, W., Yang, H. H., Jiang, S., et al. (2015). p53 loss increases the osteogenic differentiation of bone marrow stromal cells. *Stem Cells., 33*, 1304–1319.